AIP | Journal of Applied Physics

Study on the mechanical behavior of tilt bicrystal graphene by molecular dynamics simulations: Bulk verse nanoribbons

Ajing Cao and Jianmin Qu

Citation: J. Appl. Phys. **112**, 043519 (2012); doi: 10.1063/1.4749812
View online: http://dx.doi.org/10.1063/1.4749812
View Table of Contents: http://jap.aip.org/resource/1/JAPIAU/v112/i4
Published by the American Institute of Physics.

Study on the mechanical behavior of tilt bicrystal graphene by molecular dynamics simulations: Bulk verse nanoribbons

Ajing Cao[1,a)] and Jianmin Qu[1,2,b)]
[1]*Department of Civil and Environmental Engineering, Northwestern University, Evanston, Illinois 60208, USA*
[2]*Department of Mechanical Engineering, Northwestern University, Evanston, Illinois 60208, USA*

(Received 3 June 2012; accepted 9 August 2012; published online 31 August 2012)

Recent experimental studies have shown that multi-grains are ubiquitously present in graphene grown with chemical vapor deposition method technique. The potential application of the unique two-dimensional material in future nanotechnology demands full understandings of their structure and properties. Using molecular dynamics simulations, we study the mechanical response of various bicrystal graphene consisting of symmetric tilt boundary subject to uniaxial tensile loading. Both bulk graphene and graphene nanoribbons (GNRs) are studied. We revealed that nano-crack initiated at grain boundaries (GBs) leads to brittle failure with no plasticity at room temperature. The mechanism that crack nucleated at the intersection of GB and free surface followed by fast advance of crack, preventing plasticity that involves dislocation slip or GB sliding that is seen in metals. Cleavage along GBs is observed to be dominant fracture behavior in the studied GNRs. Furthermore, the ultimate tensile strength decreases with increasing vacancy concentration, illustrating that the lowered strength of GB interface is primarily due to not well-bonded atoms, shedding light to the structure-properties relationship. Finally, local strain and atomic-level stress have been shown to be able to characterize the onset of crack nucleation and thereby good quantities for predicting the resulting ultimate tensile strength. © *2012 American Institute of Physics*. [http://dx.doi.org/10.1063/1.4749812]

I. INTRODUCTION

Grain boundaries (GBs) in polycrystalline metals have been widely studied for decades.[1–3] It has been well documented that the mechanical properties of polycrystalline metals are dominantly determined by the interplay between dislocations with GBs.[4,5]

Graphene, a two-dimensional monatomic one-layer thick building block of carbon allotropes (carbon nanotube, fullerene, and diamond), has emerged as an exotic material of the upcoming century and attracted world-wide attention owing to its exceptional properties such as electronic,[6,7] thermal,[8,9] optical,[10] and mechanical properties.[11] More recently, experiments have shown that single layer graphene sheet synthesized by chemical vapor deposition (CVD) method ubiquitously contains GBs, due to the fact that metallic foil serves as a nucleation site for individual grains of graphene.[12,13]

It is well established experimentally in metals[14] and ceramics[15] that certain types of GBs can facilitate crack propagation, while others increase the resistance of crack advances. This has made it possible for GB design[16] in the way that the fracture resistance of polycrystalline materials can be optimized through the production of microstructures with a controllable distribution and arrangement of ''fracture-resistant'' boundaries. Such concept could possibly be applied to CVD-grown graphene provided that the role of specific microstructural elements on crack propagation can be well understood. The motivation of finding graphene's resistance of crack nucleation/propagation for a variety of tilt GBs drives the present study.

Atomistic simulations have been used to study the inelastic deformation mechanisms in nano-scale materials. For instance, Horstemeyer *et al.*[17] studied the length and time scale effects on the plastic flow of face-centered cubic (fcc) metals under a simple shear loading. Atomistic simulations have also been conducted to study the mechanisms of crack propagation in materials with pre-existing flaws.[18,19] These atomistic studies have provided important insight into the fracture behavior of materials with complicated structures, which is crucial for the design of stronger and tougher materials.

Although a number of studies have been conducted to study various types of point defects in single crystalline graphene,[20,21] the effects of GBs on the mechanical properties of the graphene has been lacking. Our recent study[22] on a variety of symmetric tilt GBs showed that the strength of zigzag-oriented graphene increases slightly with mis-orientation angle, while the strength of armchair-oriented graphene deceases slightly with mis-orientation angle.

In the present paper, we present a comprehensive study on the structure, energy, mechanical properties of bicrystal graphene consisting of various symmetric tilt GBs. The effects of GB mis-orientation angle, sample length, strain rate, temperature, as well as defect (vacancy) concentration on their mechanical properties are studied. The local stress and strain characterized at the critical load is used to identify the key factors controlling the strength of the GB interfaces.

The remaining part of the paper is organized as follows. Sec. II presents the modeling and simulation methodology

[a)]Present address: MST-8, Los Alamos National Laboratory, Los Alamos, New Mexico 87545, USA. Email: a-cao@northwestern.edu.
[b)]Email: j-qu@northwesetern.edu.

employed in the present study. The results on mechanical loading of armchair and zigzag-oriented bicrystals consists of symmetric tilt GB subject to uniaxial tensile loading will be presented in Sec. II. In Sec. III, discussions on the molecular dynamics (MD) results with a kinetic model are made. Furthermore, local strain and atomic-level stress is employed to characterize the onset of crack nucleation and the resulting ultimate tensile strength. Finally, major findings and summary of the results are shown in Sec. IV.

II. MODELING

In the present study, reactive empirical bond order (REBO) potential[23] was employed. REBO potential has been shown to accurately capture the bond-bond interaction between carbon atoms as well as bond breaking and bond reforming.

A. Constructing GB structure

To construct various symmetric tilt GB structures, we have developed a scheme as follows:

(1) A periodicity cell length of L_x and L_y was first determined by tilting the two bicrystal grains to the desired angles with respect to each other.
(2) Two tilted grains with desired crystallographic orientations were put together with a small gap smaller than 0.2 Å, depending on the specific structure.
(3) A *NPT* (number of atoms N, pressure P, and temperature T are conserved) ($P = 0.1$ GPa and $T = 300$ K) run followed by a *NVT* (number of atoms N, volume V, and temperature T are conserved) run was performed to relax the initial as-prepared configurations.
(4) If other than perfect three-coordinated atoms exist, a new atom was deposited around the non-three coordinated atom at the GB region.
(5) The repeating process of 1∼4 continued until all atoms were of coordination number 3.

Although in theory that all tilt angles are possible for constructing GBs, we found there are a few that are able to build up symmetric tilt GBs, which are the focus of the present study. The enumeration of all possible tilt GBs seems to be a challenging task and in principle intractable. Nevertheless, the list of symmetrical tilt mis-orientation angle GBs we found is shown in Table I.

TABLE I. The mis-orientation angles and GB energy of the zigzag and armchair-oriented bicrystal graphene studied in the present work.

Type of GB	GB energy (eV/Å)	Type of GB	GB energy (eV/Å)
Zigzag-oriented		Armchair-oriented	
5.5°	0.021	15.18°	0.612
9.8°	0.720	17.9°	0.751
13.2°	0.234	21.4°	0.702
16.43°	0.620	28.7°	0.637
17.9°	0.707	36.8°	0.707
21.7°	0.300	42.6°	0.757
32.5°	0.332	50.2°	0.671

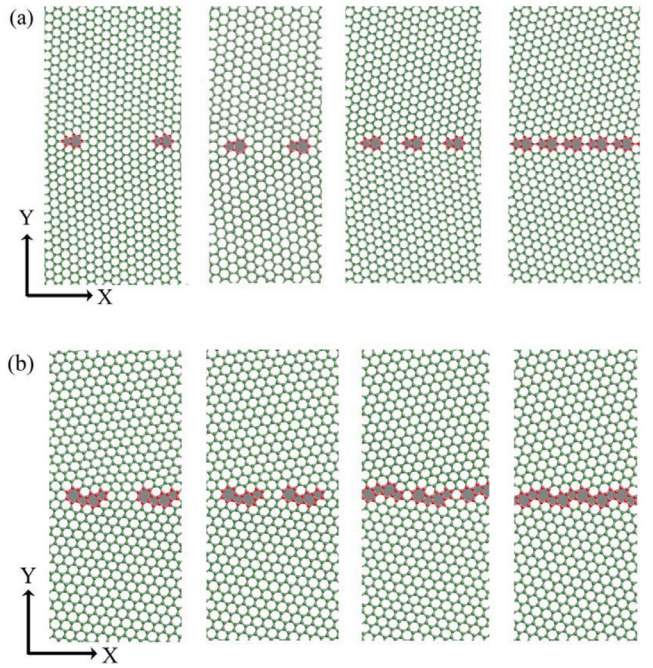

FIG. 1. The typical structure of GBs in the as-prepared (a) zigzag-oriented graphene (5.5°, 9.8°, 13.2°, and 21.7°). (b) Armchair-oriented graphene (15.18°, 17.9°, 21.4°, and 28.7°).

It is worth noting that our constructed 5.5° armchair-oriented graphene has a repeat unit of separated by 7 and 9 hexagonal rings (see Figure 1), which is different from the model in Ref. 24. In addition, we were not able to construct 15.8° armchair-oriented graphene, instead we found 15.18° is a stable one, which is shown in Figure 1 as well.

The structures of the symmetric tilt GBs in zigzag and armchair-oriented tilt bicrystals are shown in Figures 1(a) and 1(b), respectively. The GBs consist of repeating five- and seven-membered ring pairs (5–7 pairs) that are separated by several hexagonal rings. It is observed that the number of hexagonal rings separating the 5–7 defects decreases as the mis-orientation angle increases, with the limit occurring at 21.7° in which only a single hexagonal ring separates the periodic 5-7 defects in the zigzag-oriented graphene. Likewise, in the armchair-oriented graphene, 28.7° is the highest defect density case as 5-7 ring pairs are the only components in the GBs. Therefore, the trend is clear in the two cases: bicrystals with larger GB tilt angles are composed of higher defect densities. The repeating defect pairs can also be thought of as an array of edge dislocations with horizontal Burgers vectors where the five-membered rings represent the extra plane of atoms. To be specific, the defects can be categorized into two types of dislocations, namely (1,0) and (1,0) + (0,1) dislocation pair. The most common GBs consist of repeating pentagon and heptagon pairs (5-7 pairs) that are separated by several hexagonal rings, as shown in Figure 1(a). The other type is (1,0) dislocation, which is repeated five-and seven-membered ring. It should be pointed out that the (1,0) + (0,1) dislocation pair is generally lower than the (1,0) type of dislocation. These structural irregularities are thought to be the weak phase and potential crack nucleation sites, which deserve detailed analysis as will be shown in Sec. IV.

B. GB energy

The GB energy γ was computed as

$$\gamma = \frac{N(E_{total} - E_{pristine})}{2L}, \quad (1)$$

where N denotes the number of total atoms in the system; L being the length of the simulation cell, E_{total} being the potential energy per atom of the system with GBs and $E_{pristine}$ being the potential energy per atom of the pristine graphene.

The energy associated with various types of GBs as a function of mis-orientation angle is shown in Figure 2. The result shows that some low angle zigzag-oriented bicrystals have relatively lower GB energies. Interestingly, the 5.5° zigzag-oriented bicrystal has the lowest GB energy, 0.02 eV/Å, which is one order of magnitude lower than that of other GBs. Also is evident is that the zigzag-oriented GB generally has lower energy than that of armchair-oriented GB, with a few exceptions such as 9.8°, 16.43°, and 17.9°. From structure point of view, higher angle GBs generally corresponds to larger defect density per unit area, as we observed here.

C. Mechanical behavior of bulk graphene

To study the mechanical properties of bulk graphene, the bicrystals were subjected to periodic boundary conditions (PBCs) in the two in-plane dimensions. The loading scheme was as follows: a coupled *NPT* ensemble ($P = 0$ GPa) with a constant uniaxial strain rate loading scheme was employed. Specifically, a constant strain rate was adopted in the X direction and boundary condition in Y direction was specified as stress-free. Strain was introduced by uncoupling the unit cell vector along the X direction and extending it during the simulations according to the applied strain rate.

The stress-strain (σ-ε) curves of a variety of bulk bicrystals are shown in Figure 3. The engineering strain and Cauchy stress were used. In calculating the Cauchy stress, it was assumed that the thickness of the graphene remains at the nominal thickness of 0.34 nm (interlayer thickness of graphite) during the deformation process, while the width

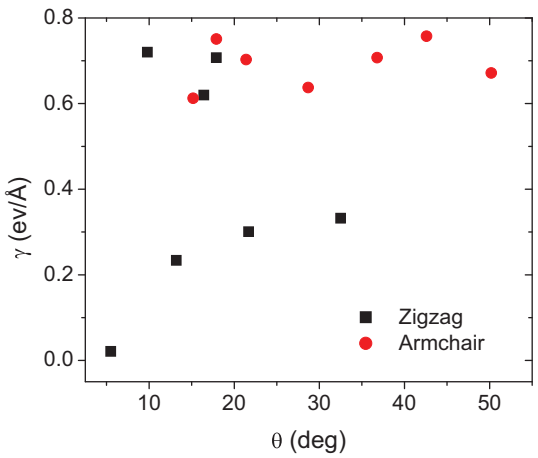

FIG. 2. The GB energy in the two set of bicrystal graphene as a function of mis-orientation angle.

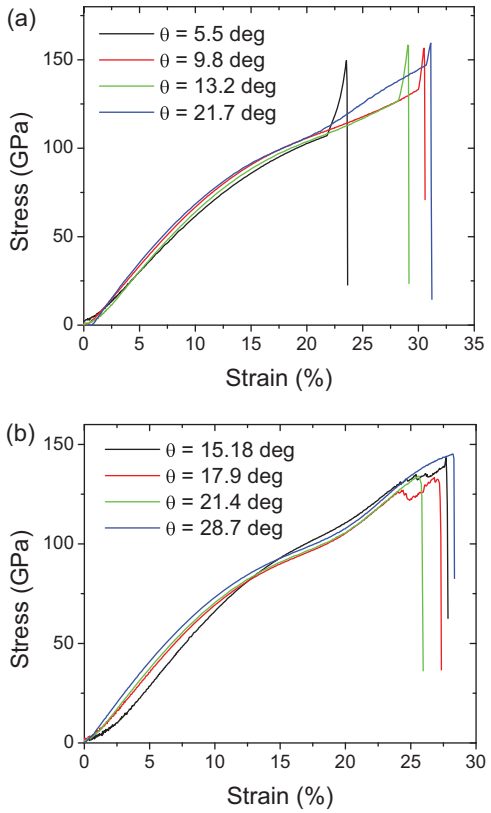

FIG. 3. The stress-strain curves of various bicrystal bulk graphene at a strain rate of $1 \times 10^9\ s^{-1}$. The size of samples is 8 nm × 8 nm. (a) Zigzag-oriented bicrystal and (b) armchair-oriented bicrystal.

(Y-direction) was allowed to shrink freely. It is seen from Figure 3 that, for all the samples, the stress-strain relationship remains linear up to ~5%, and becomes nonlinear beyond 5%. The ultimate tensile strengths defined as the maximum stress in the stress-strain curve in both armchair and zigzag-oriented bulk bicrystals are larger than 125 GPa, ranging from 125 to 148 GPa, and from 145 to 158 GPa, respectively. Interestingly, the bicrystal samples start to fail at strains corresponding to the points at which precipitous drop occurs in the stress-strain curves. It is also observed that all the studied zigzag-oriented bicystal show strong hardening effects close to the failure point.

It should be noted that PBCs were imposed on both in-plane directions to model bulk graphene. This corresponds to homogeneous nucleation of crack in an infinitely large sample. In analogous of homogeneous nucleation of dislocation in single crystal metals (in absence of any heterogeneities such as free surfaces, grain boundaries, phase boundaries, structure defects, etc.), the stress required for such homogenous nucleation is much higher than that for heterogeneous nucleation such as cases with GBs and free surfaces as will be shown in graphene nanoribbon (GNR) cases.

The snapshots of bulk 21.4° armchair-oriented bulk graphene close to failure are shown in Figure 4. Apparently, the onset of instability is dictated by nano-voids nucleation. It is observed that multiple voids (pointed by dashed black circles) nucleated both at GB region and grain interior simultaneously.

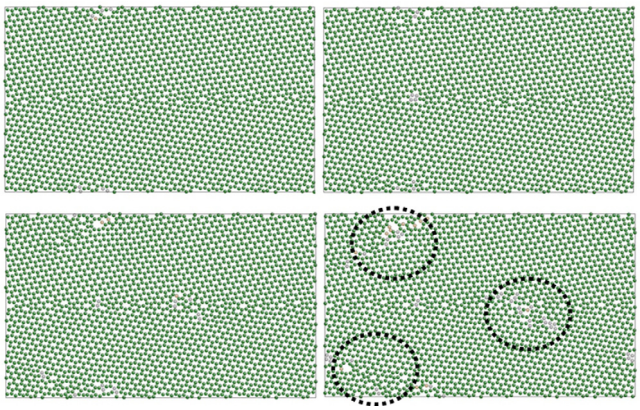

FIG. 4. A consecutive snapshots showing the onset of instability dictated by nano-voids nucleation occurring at a 21.4° armchair-oriented bulk graphene (PBC were imposed at both X and Y directions). It is observed that multiple voids (pointed by dashed black circles) nucleated both at GB region and grain interior simultaneously.

D. Mechanical behavior of GNRs

To study the mechanical behavior of GNRs, we have tried two loading schemes: (1) The two ends of GNRs were fixed in all three directions and one end was pulled with a constant velocity, which results in a constant engineering strain rate of 0.5 ps^{-1}. (2) The two ends of GNRs were fixed in the loading direction but were allowed to move in the lateral directions. Then, the two ends were pulled in a constant velocity along the direction perpendicular to the GB interface, which results in a constant engineering strain rate of 0.5 ps^{-1}. The difference between the two loading schemes was that for the first case, the stress near the fixed ends has built up shear strain, while the second one yields a uniform strain in the entire system.

As a representative example, the stress-strain curves for a 15.18° armchair-oriented GNRs with sizes of 16 nm × 16 nm are shown Figure 5 in using both two methods. It appears that inappreciable difference between the two stress-strain curves can be detected.

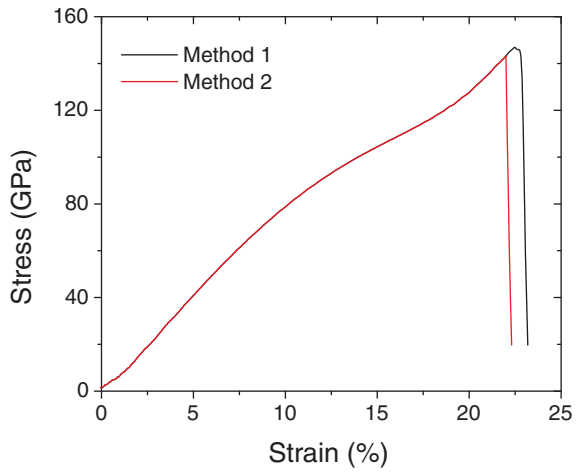

FIG. 5. The stress-strain curves using the two methods with different boundary conditions.

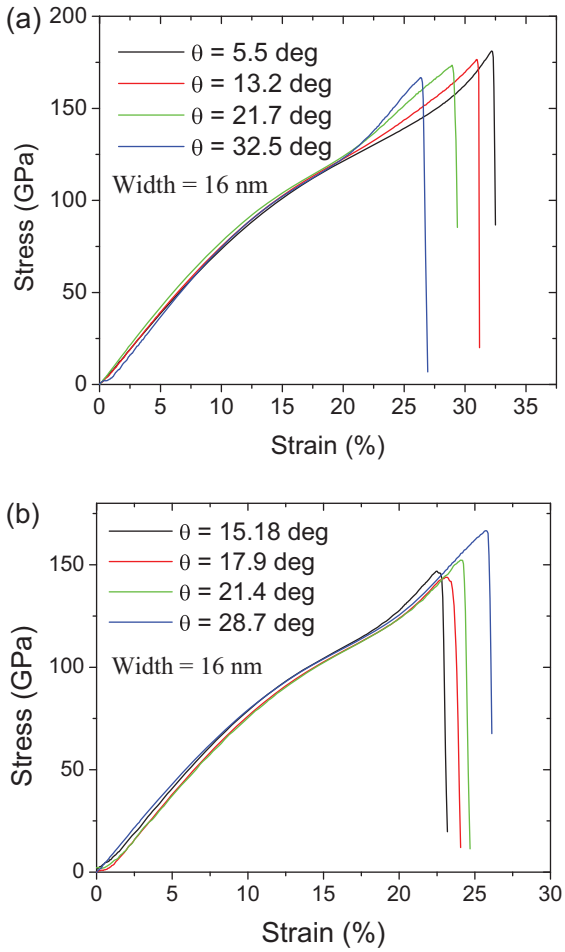

FIG. 6. The stress-strain curves of various bicrystal GNRs at a strain rate of $1 \times 10^9\ s^{-1}$. The size of samples is 16 nm × 16 nm. (a) Zigzag-oriented bicrystal and (b) armchair-oriented bicrystal.

The stress-strain curves of a variety of bicrystals GNRs are shown in Figure 6. It is seen from that, for all the samples, the stress-strain relationship remains linear up to ~5%, and the difference in Young's modulus is inappreciable. It appears that the ultimate tensile strength of zigzag-oriented GNRs increases with mis-orientation angle while the strength of armchair-oriented GNRs decreases with mis-orientation angle. The variation of ultimate tensile strength for all the studied bicrystal GNRs ranges from 145 GPa to 180 GPa, which is much smaller than what has been reported in Ref. 24.

In the GNR cases, due to the presence of free surfaces, the dangling atoms at the surface edges are more prone to deform. The deformation snapshots close to failure of the 21.4° armchair-oriented graphene bicrystal GNR are shown in Figure 7. The movie of the entire deformation process is shown in supplemental mater movie.[37] As shown, the crack is nucleated at the GB followed by quick advance of the crack, leading to cleavage failure.

Due to the high surface to volume ratio in GNRs, there is always concern regarding whether or not the free surface plays an important role in their mechanical properties, like in metallic[25,26] and semiconductor nanowires.[27] Here, as a representative, we choose 13.2° zigzag-oriented GNRs with

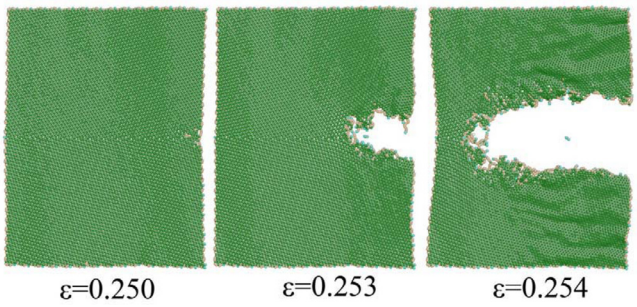

FIG. 7. A consecutive snapshots showing the fracture process of a 21.4° armchair-oriented GNR. The brittle failure is initiated by nucleating nanocrack at GBs followed by quick growth of the crack.

size of 4 nm, 8 nm, and 16 nm. The results are shown in Figure 8. The stress-strain curves overlaps and the ultimate tensile strength is almost the same. This seems to suggest that the lateral size effect on the ultimate tensile strength is negligible beyond 16 nm.

E. Strain rate effects

High strain rate sensitivity has been found in nanocrystalline metals[28,29] and polymer.[30] In the section, we have carried out simulations on several cases with different strain rates. In contrast to other strain-rate dependent materials, in which higher plastic yielding stresses were found at higher strain rates in many previous studies,[31,32] the mechanical properties of bicrystal graphene are less dependent on strain rate. The reason is that the ultimate tensile strength seen in bicrystal graphene is not dominated by plastic yielding. In contrary, the mechanism that dictates fracture in graphene is atomic bond breaking followed by catastrophic brittle fracture with no plasticity. Due to the fundamental difference in failure/yielding mechanisms, the strain rate sensitivity of ultimate tensile strength in graphene is different to that of plastic yielding in metals.

Figure 9 shows the strain rate effect on the stress-strain response of the 13.2° zigzag-oriented bicrystal GNRs. It can be observed that the three curves overlap and difference among them is inappreciably small, showing no rate effects of Young's modulus and quite small variation of ultimate tensile strength due to strain rate effects.

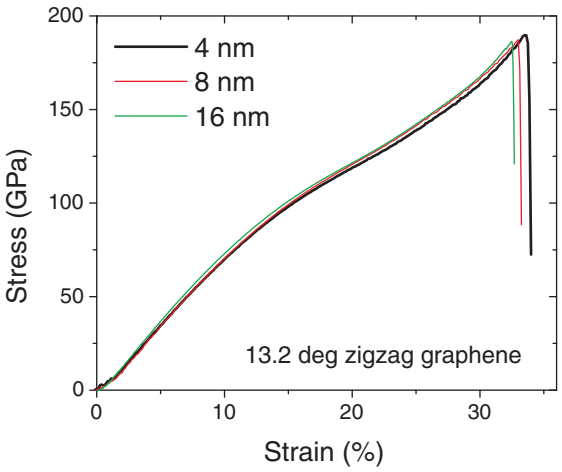

FIG. 8. The stress-strain curves of 13.2° zigzag-oriented GNRs of different sizes, showing unnoticeable size effects on the tensile stress-strain curves.

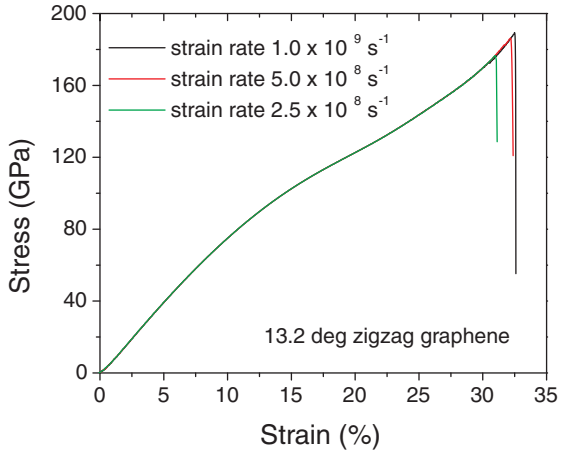

FIG. 9. The strain rate effect on the stress-strain response of the 13.2° zigzag-oriented bicrystal GNRs. The three curves overlap and difference among them is inappreciable small, showing no rate effects of Young's modulus and quite small variation of ultimate tensile strength due to strain rate effects.

F. Temperature effects

Owing to wide range working conditions, graphene will be working on, such as high temperatures, large electricity fluxes, etc., it is of great interest to gain knowledge on the mechanical behavior under various working conditions. For this purpose, the uniaxial tensile loading of bicrystal graphene was performed at different temperatures. A representative stress-strain result for the 21.7° zigzag-oriented graphene is shown in Figure 10(a). Clearly, Young's modulus decreases monotonically with temperature. This is similar to other materials like metals.[32,33] Also is evident is that the ultimate tensile strength decreases with increasing temperature. The weak temperature dependence on strength is probably due to the nature of chemical C-C bond, although the activated process of bond breaking at the fracture strain becomes a rate dependent process. In contrast, a strong temperature dependence on yield strength at cryogenic temperatures has been found for nanocrystalline Ni,[34] which was attributed to the small dislocation activation volume from GBs at small grain sizes. Further discusses will be presented in Sec. IV.

G. Vacancy concentration effects

Since the exact atomic-level GB structure may vary with the graphene synthesis techniques, it is also helpful to understand how the mechanical properties vary with the defect concentrations. Here, we model the GB structure by removing a certain number of atoms at GB region in a periodic fashion (per unit box length). As shown in Figure 11, a desired amount of atoms were chosen to be deleted, and the vacancy concentration was calculated with respect to that with no vacancies.

The resulting stress-strain curves are shown in Figure 12. Compared to the bicrystal graphene without vacancies,

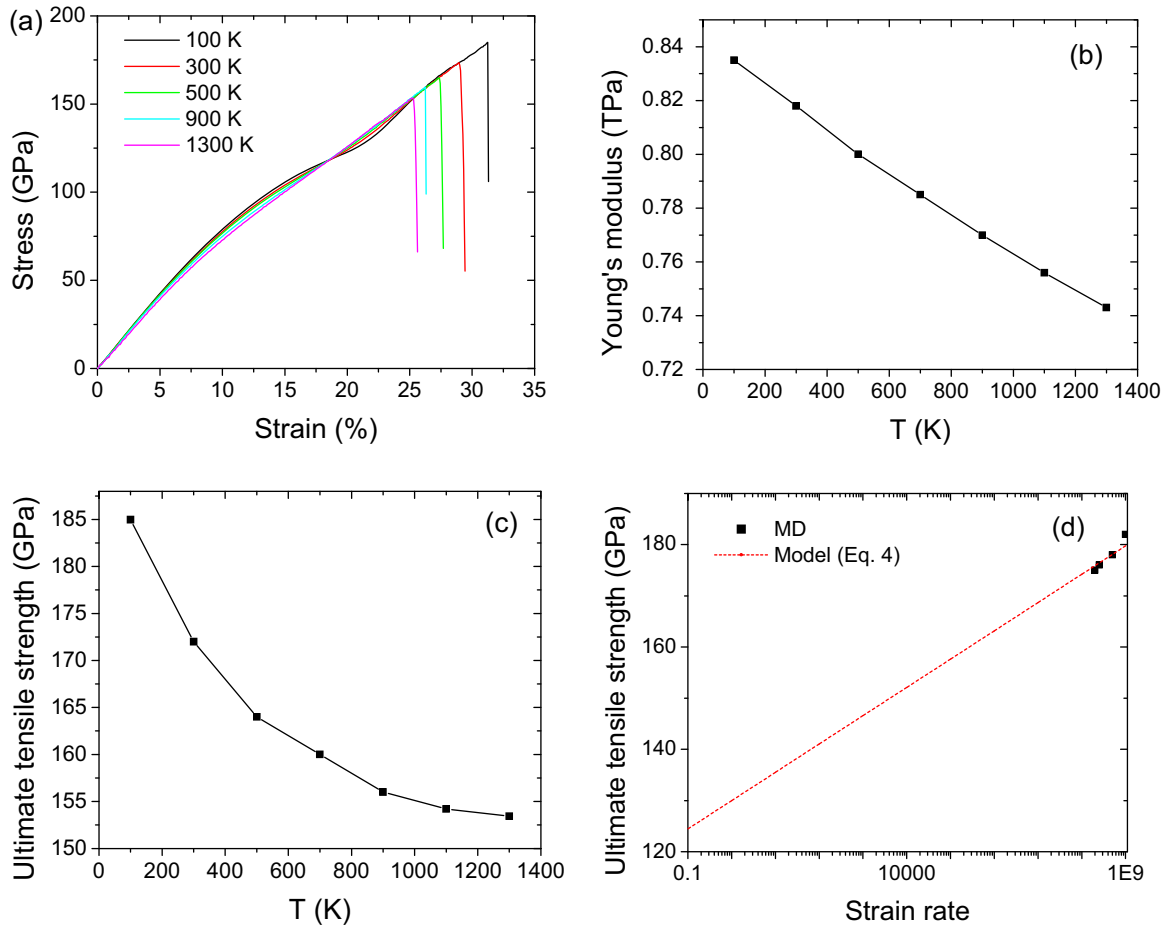

FIG. 10. The stress strain curve under various temperatures. (a) The stress-strain curves for the 21.7° zigzag-oriented bicrytal GNRs under various temperatures. (b) The modulus as a function of temperature. (c) The ultimate tensile strength as a function of temperature. (d) The extrapolation of strength at low strain rates from our MD data at high strain rates.

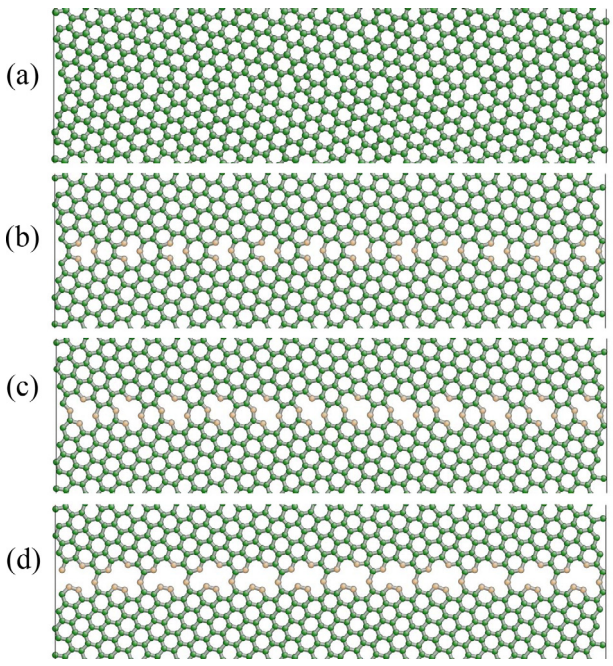

FIG. 11. The configurations of 21.7° zigzag-oriented bicrystal graphene with different vacancy concentration. The bulk atoms are shown in green and brown represents defective atoms. (a) no vacancy, (b) 1 vacancy, (c) 2 vacancies, and (d) 3 vacancies per unit box length (0.6 nm).

bicrystal graphene have higher vacancy concentration show lowered ultimate tensile strength. The overall trend is that the more defects (vacancies) the sample contains, the smaller the strength it has. The result illustrates that the lowered strength of GB interface is primarily due to the not well-bonded atoms. Also, due to the presence of vacancies, the load-transfer in the materials is altered. For example, some

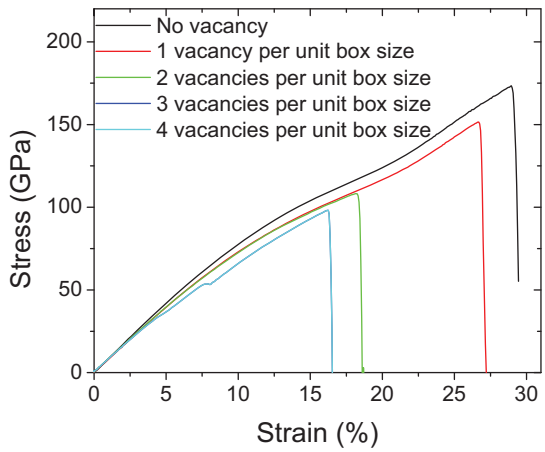

FIG. 12. The stress-strain curves of 21.7° zigzag-oriented bicrystal GNRs that consists of a certain amount of vacancies at GBs. The unit box length of the 21.7° zigzag-oriented bicrystal GNR is 0.6 nm.

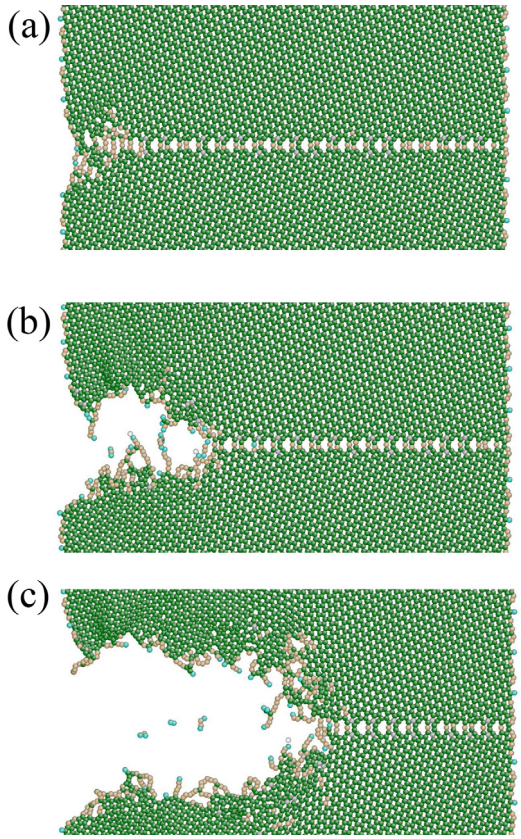

FIG. 13. The snapshots right before failure for the 21.7° zigzag-oriented graphene that contains 1 vacancy per unit box length (0.6 nm). Clearly, the advancement of crack leads to cleavage along the GB and consequent failure of the material.

missing atoms do not carry loads and thereby the Young's modulus is reduced for the bicrystal graphene.

Figure 13 shows the deformation snapshots right before failure for the 21.7° zigzag-oriented graphene that contains 1 vacancy per unit box length (0.6 nm). Clearly, the advancement of crack leads to cleavage along the GB and consequent failure of the material. The same behavior is also observed for other samples with different vacancy concentrations.

III. DISCUSSIONS

A. Strain rate sensitivity

To gain further insight on the rate sensitivity of the brittleness of graphene, we have attempted to circumvent the issue with a kinetic model. The Arrhenius formulation[35] that relates the lifetime τ as a function of tensile stress σ and temperature T was adopted in our analysis

$$\tau = \frac{\tau_0}{n_s}\exp\left(\frac{U_0 - \gamma\sigma}{k_B T}\right), \tag{2}$$

where τ_0 is the vibration period of atoms, n_s is defined as the number of sites available for the state transition, U_0 is the inter-atomic bond breaking energy, and $\gamma = qV$, where V is the activation volume and q is the coefficient of local overstress, and k_B is the Boltzmann constant. The lifetime τ, defined as the time taken for a stressed solid to breakdown, is directly related to the energy barrier $U_0 - \gamma\sigma$, and temperature T, by the Maxwell–Boltzmann distribution. The energy barrier for bond breaking is typically lowered by the applied tensile stress and thermal motion of atoms.

In the constant strain rate loading process like what we have modeled here, the stress $\sigma(t)$ is related to the strain rate by $\sigma = E\dot{\varepsilon}t$, where E denotes the apparent Young's modulus of graphene.

Apparently, the activation volume of bond breaking is small, in the range of $\sim$nm^2, The fracture stress given by Eq. (2) is then can be rearranged as[31]

$$\sigma(\dot{\varepsilon}) = \frac{Q^*}{\Omega} - \frac{k_B T}{\Omega}\ln\frac{k_B T N \nu_0}{E\dot{\varepsilon}\Omega}. \tag{3}$$

Here, the first term is the athermal nucleation stress causing instantaneous crack nucleation in the linearized model of stress-dependent activation energy. The prefactor of the second term sets the scale of nucleation stress reduction due to thermal fluctuation. In the logarithmic function, $k_B T N \nu_0$ is the rate of energy exchange of the candidate nucleation sites with the thermal bath, and $E\dot{\varepsilon}\Omega$ is the rate of activation energy reduction by the mechanical work.

Since we do not know what values of Q^* and Ω are, we set with two unknown parameters

$$\sigma(\dot{\varepsilon}) = C0 - C2\ln\frac{C3}{\dot{\varepsilon}} = C0 + C1\ln\dot{\varepsilon}. \tag{4}$$

The best fit of the MD data with two free parameters ($C0$ and $C1$) of Eq. (4) is shown in Figure 10(d). The extracted fracture strength at strain rate of 0.1 s^{-1} is $\sim$125 GPa, showing rather small strain rate sensitivity. The rough estimation gives us the idea that the fracture stress is still high even if the strain rate is in the order of experimental values ($\sim 10^{-1}$ s^{-1}) and the strain rate sensitivity of fracture strength is weak.

B. The criterion on crack nucleation and consequent brittle failure

The above shows the MD results for a variety of bicrystals. It is clear that brittle fracture is the dominant deformation mode. Once crack is nucleated, the graphene has no further resistance to crack propagation under such high stress and the material quickly fails. Therefore, crack nucleation is the key mechanical instability to characterize the ultimate tensile strength of graphene. One question naturally arises: Can we establish a general criterion for the onset of crack nucleation that determines the ultimate tensile strength of the bicrystal graphene? In the following, we attempt to explain the observed simulation results by charactering the crack nucleation with two local probing.

1. Strain characterization

The atomic-level strain employing the atomic positions at any moment was used to characterize the local strain. The original perfect hexagonal structure was adopted as the reference structure.

The local Lagrangian strain at atom i is defined to be

$$\eta = \frac{1}{2}(\mathbf{J}^T\mathbf{J} - \mathbf{I}) \tag{5}$$

and the local shear strain invariant (SSI) is[32]

$$\eta_s = \sqrt{\frac{1}{2}Tr(\eta - \eta_m\mathbf{I})^2}, \tag{6}$$

where $Tr(\mathbf{A})$ is the trace of the tensor $\mathbf{A}$. After obtaining η_{si} for all atoms, one may also compute system average η_{save} and evaluate local deviations from η_{sdev}.

We found that the local SSI is a good diagnostic method for predicting the nano-crack nucleation. The SSI in the 21.4° armchair-oriented graphene GNR is shown in Figure 14. Right before the embryonic nano-crack nucleation ($\varepsilon = 0.245$, Figure 14(b)), the largest strain occurs at the site that the embryonic nano-crack is nucleated. Then, it is worthwhile to see what strain distribution is in the initial configuration. As shown in Figure 14(a), the local strain at GB is indeed larger than other places in the grain interior.

2. Stress characterization

The atomic-level stress is defined as

$$\sigma_i^{\alpha\beta} = \frac{1}{\omega_i}\left[-\frac{1}{2}m_i v_i^\alpha v_i^\beta + \sum_{j\neq i} f_{ij} r_{ij}^\alpha r_{ij}^\beta\right], \tag{7}$$

where $\sum \omega_i = \Omega$, ω_i is taken as the effective volume of the atom i, Ω is the volume of the system. m_i and v_i are the mass and velocity of atom i, the indices α and β denote the Cartesian components, and r_{ij} and f_{ij} are the distance and force between atoms i and j, respectively. The same method has been used for bicrystal metal nanowires in our previous work.[36]

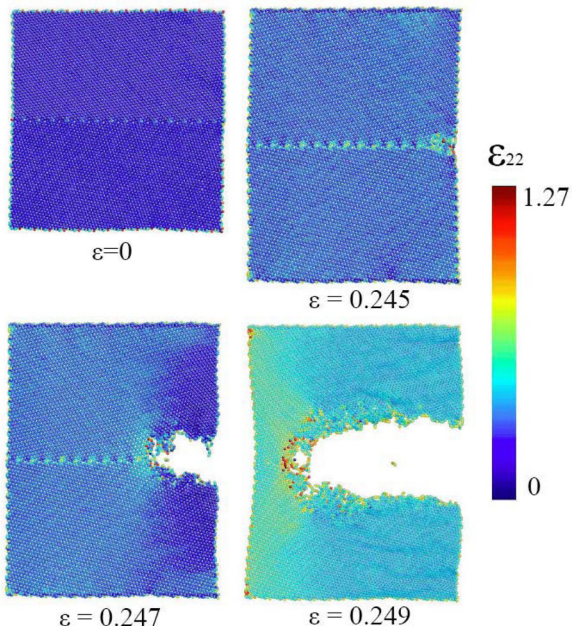

FIG. 14. The local strain characterization in the 21.4° armchair-oriented GNR. (a) Owing to the non-perfect structure at the GB region *albeit* of the same coordination number as bulk atoms, the local strain in the initial configuration is larger at GB region. (b) At strain of 0.245, the strain at GB region becomes more heterogeneous. (c) The crack nucleated and the strain at crack tip is of the largest value. (d) The crack moves along the GB and strain at the crack tip is shown the largest value.

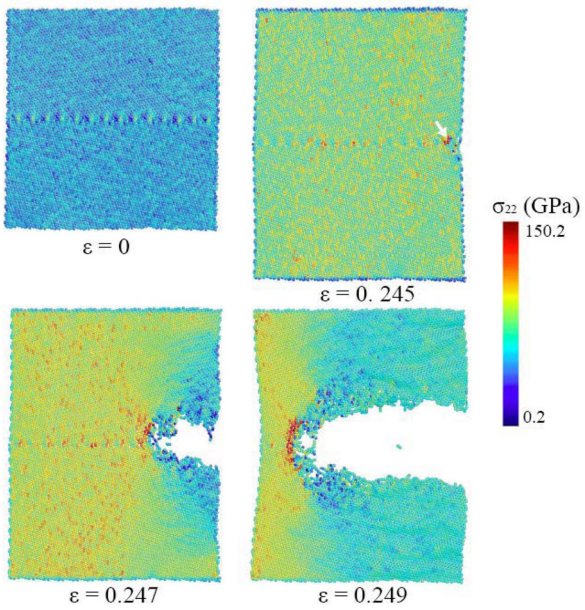

FIG. 15. The atomic-level stress characterization in the 21.4° armchair-oriented GNR. (a) In the initial configuration ($\varepsilon = 0$), the residual stress at the GB in the middle is heterogeneous while stress in the grain interior is more uniform. (b) At the moment that embryonic nano-crack nucleates (pointed by the white arrow) ($\varepsilon = 0.245$), the largest stress is found at the same embryonic nano-crack nucleation location at the GB region. (c) The crack advance along the GB. (d) After the crack front moves, the stress in the right part is released. Clearly, stress concentration ahead of crack tip is observed.

Figure 15(a) shows that the stresses are quite uniform in the grain interior far from the GBs at $\varepsilon = 0$. The distribution of the heterogeneous interface stress in the GB region, which directly results from the large fractions of not well-bonded atoms at the GBs, is believed to be the origin of lowered strength for bicrystal GNRs. The maximum stress is ~2.0 GPa, By averaging the stress component σ^{22} over the atoms in the GB region, the average is 0.82 GPa. Meanwhile, the stress at the interior at the initial equilibrium state is ~0 Gpa. The stress increases with the applied strains. When the strain reaches 0.245, an embryonic nano-crack nucleates from the GB region, as shown in Figure 15(b). Here, interestingly, we found the stress at the embryonic nano-crack location is the maximum, which indicates that the local region has reached the threshold that C-C bonds can sustain. Therefore, instability dictated by bond-breaking occurs at the local region. Once the crack is initiated, stress redistribution at the crack tip take place immediately and crack propagation under such high stress occurs quickly causing brittle failure. Based on the above analysis, we believe the residual stress due to the presence of GB is the origin of lower fracture strength of the bicrystal GNRs and GB can be viewed as "weak phase" in graphene.

IV. CONCLUDING REMARKS

The structure and mechanical properties of bicrystal graphene consists of symmetric tilt GBs have been systematically

studied with MD simulations. Our comprehensive models of a variety of armchair and zigzag-oriented graphene show that GB energy varies ranging from 0.02 to 0.75 eV/Å. In general, armchair-oriented GBs show higher GB energy than zigzag-oriented GBs. Mechanical response of bulk graphene and GNRs subject to uniaxial tension is studied. Cleavage along GB is observed in GNRs leading to brittle failure. Crack nucleation at the intersection of GB and free surface followed by fast advance of crack under high stress, preventing plasticity that involves dislocation slip or GB sliding that is seen in metals. Furthermore, the ultimate tensile strength decreases with increasing vacancy concentration, illustrating the weakness of GB interface is primarily due to not well-bonded atoms. Our study thereby shed lights on the structure-property relationship of graphene with certain types of GBs. The results have implications for tuning graphene's micro-structure to achieve the desired mechanical properties. In the end, considering the small variation of ultimate tensile strength with mis-orientation angle, we conclude that the ultimate tensile strength of graphene with symmetric tilt GBs is insensitive to the tilt mis-orientation angle.

ACKNOWLEDGMENTS

We gratefully acknowledge for the use of QUEST cluster at Northwestern University.

[1]H. Gleiter, Prog. Mater. Sci. **33**, 223 (1989).
[2]M. A. Meyers, A. Mishra, and D. J. Benson, Prog. Mater. Sci. **51**, 427 (2006).
[3]K. S. Kumar, H. Van Swygenhoven, and S. Suresh, Acta Mater. **51**, 5743 (2003).
[4]E. O. Hall, Proc. Phys. Soc. London, Sec. B **64**, 747 (1951).
[5]N. J. Petch, J. Iron Steel Inst. **174**, 25 (1953).
[6]A. K. Geim and K. S. Novoselov, Nature Mater. **6**, 183 (2007).
[7]A. K. Geim, Science **324**, 1530 (2009).
[8]A. A. Balandin, S. Ghosh, W. Z. Bao, I. Calizo, D. Teweldebrhan, F. Miao, and C. N. Lau, Nano Lett. **8**, 902 (2008).
[9]A. Cao and J. Qu, J. Appl. Phys. **111**, 053529 (2012).
[10]K. F. Mak, M. Y. Sfeir, Y. Wu, C. H. Lui, J. A. Misewich, and T. F. Heinz, Phys. Rev. Lett. **101**, 196405 (2008).
[11]C. Lee, X. D. Wei, J. W. Kysar, and J. Hone, Science **321**, 385 (2008).
[12]P. Y. Huang, C. S. Ruiz-Vargas, A. M. van der Zande, W. S. Whitney, M. P. Levendorf, J. W. Kevek, S. Garg, J. S. Alden, C. J. Hustedt, Y. Zhu, J. Park, P. L. McEuen, and D. A. Muller, Nature (London) **469**, 389 (2011).
[13]K. Kim, Z. Lee, W. Regan, C. Kisielowski, M. F. Crommie, and A. Zettl, ACS Nano **5**, 2142 (2011).
[14]T. Watanabe, Mater. Sci. Eng., A **176**, 39 (1994).
[15]G. Palumbo and K. T. Aust, edited by D. Wolf and S. Yip, *Materials Interfaces* (Chapman & Hall, London, 1992), p. 190.
[16]L. C. Lim and T. Watanabe, Acta Metall. Mater. **38**, 2507 (1990).
[17]M. F. Horstemeyer, M. I. Baskes, and S. J. Plimpton, Acta Mater. **49**, 4363 (2001).
[18]F. F. Abraham and H. J. Gao, Phys. Rev. Lett. **84**, 3113 (2000).
[19]S. J. Zhou, D. M. Beazley, P. S. Lomdahl, and B. L. Holian, Phys. Rev. Lett. **78**, 479 (1997).
[20]Q. X. Pei, Y. W. Zhang, and V. B. Shenoy, Carbon **48**, 898 (2010).
[21]J. R. Xiao, J. Staniszewski, and J. W. Gillespie, Mater. Sci. Eng., A **527**, 715 (2010).
[22]A. J. Cao and Y. T. Yuan, Appl. Phys. Lett. **100**, 211912 (2012).
[23]D. W. Brenner, O. A. Shenderova, J. A. Harrison, S. J. Stuart, B. Ni, and S. B. Sinnott, J. Phys. Condensed Matter **14**, 783 (2002).
[24]R. Grantab, V. B. Shenoy, and R. S. Ruoff, Science **330**, 946 (2010).
[25]H. Y. Liang, M. Upmanyu, and H. C. Huang, Phys. Rev. B **71**, 241403(R) (2005).
[26]K. Gall, J. K. Diao, and M. L. Dunn, Nano Lett. **4**, 2431 (2004).
[27]M. J. Gordon, T. Baron, F. Dhalluin, P. Gentile, and P. Ferret, Nano Lett. **9**, 525 (2009).
[28]L. Lu, R. Schwaiger, Z. W. Shan, M. Dao, K. Lu, and S. Suresh, Acta Mater. **53**, 2169 (2005).
[29]R. J. Asaro and S. Suresh, Acta Mater. **53**, 3369 (2005).
[30]Z. H. Li and J. Lambros, Int. J. Solids Struct. **38**, 3549 (2001).
[31]T. Zhu, J. Li, A. Samanta, A. Leach, and K. Gall, Phys. Rev. Lett. **100**, 025502 (2008).
[32]A. Cao and E. Ma, Acta Mater. **56**, 4816 (2008).
[33]Y. A. Chang and L. Himmel, J. Appl. Phys. **37**, 3567 (1966).
[34]Y. M. Wang and E. Ma, Appl. Phys. Lett. **85**, 2750 (2004).
[35]S. Arrhenius, Z. Phys. Chem. **4**, 226 (1889).
[36]A. Cao, Y. G. Wei, and E. Ma, Phys. Rev. B **77**, 195429 (2008).
[37]See supplementary material at http://dx.doi.org/10.1063/1.4749812 for the entire deformation process of the 21.4° armchair-oriented graphene bicrystal GNR.